Utility of Modular Attitude Determination and Control Subsystems for Small Satellites

Christopher P. Lomanno and Robert A. Bettinger
Air Force Institute of Technology, Wright-Patterson Air Force Base, OH
Paul Gindre
École de l'Air, Salon-de-Provence, France

ABSTRACT

The viability of using multiple small commercial-off-the-shelf (COTS) attitude determination and control systems (ADCS) is investigated to improve the performance of a 6U CubeSat. The ADCS represents one of the most complex CubeSat subsystems, which usually impels spacecraft developers to purchase a COTS unit rather than endeavor to develop a unique subsystem to fulfill mission requirements. CubeSat-sized ADCS are typically manufactured to measure 0.5U and output a maximum of 900 mN·m of torque. Consequently, CubeSat developers using larger busses routinely utilize an ADCS with undersized reaction wheels for control of their spacecraft. This research analyzes the benefits and costs of using two identical but independent COTS attitude control units, with each being closed-loop systems that behave independently while being fixed inside the same rigid body. For the present research, we use a software-based system model of the Blue Canyon Technologies' XACT as the COTS ADCS, which utilizes 4 reaction wheels in a pyramidal array. For the system model, the attitude control unit parameters use a quaternion feedback regulation control law consisting of linear feedback of error quaternions and body rates, with initial conditions set with a rotation and symmetric wheel speed configurations. Overall, control features like slew rates, settling times, and energy usage are investigated using various placements and orientations of the attitude control units with respect to each other inside a 6U CubeSat chassis.

NOMENCLATURE

c_i	=	direction cosines of Euler axis relative to reference frame
$\mathbf{D}, \mathbf{K}$	=	gain matrices, $(\mathrm{kg} \cdot \mathrm{m})/\mathrm{s}$
E_i	=	energy used by each reaction wheel, J
$\mathbf{h_i}$	=	momentum of reaction wheel about spin axis, $(\mathrm{kg} \cdot \mathrm{m})/\mathrm{s}$
$[\mathbf{I}]$	=	spacecraft inertia tensor, $\mathrm{kg} \cdot \mathrm{m}^2$
$[\mathbf{J}]$	=	torque distribution matrix, $1/(\mathrm{kg} \cdot \mathrm{m}^2)$
$\mathbf{M}$	=	motor location in chassis
M_{inv}	=	largest invariant set for LaSalle analysis
$\mathbf{MB}$	=	motor to body torque distribution matrix, $\mathrm{kg} \cdot \mathrm{m}^2$
$\mathbf{q}$	=	attitude quaternion in body frame
$\mathbf{q_c}$	=	commanded quaternion
$\mathbf{q_e}$	=	quaternion error
$\mathbf{R_i}$	=	rotation matrix
S	=	wheel saturation speed, rev/s
t_s	=	settling time, s
$\mathbf{u}$	=	system control torque, $\mathrm{N} \cdot \mathrm{m}$
$\mathbf{u_{s_i}}$	=	motor torques of the *i*th wheel, $\mathrm{N} \cdot \mathrm{m}$
V	=	Lyapunov candidate function
$\boldsymbol{v_i}$	=	motor rotational speeds of the *i*th wheel, rev/s
W	=	wheel inertia, $\mathrm{kg} \cdot \mathrm{m}^2$
X_d	=	attitude control unit spatial position, m
X_r	=	attitude control unit axis orientation
ζ	=	damping ratio
Ω_i	=	rotational velocity of reaction wheel about spin axis relative to spacecraft, m/s
θ	=	rotation angle for rotation matrix, rad
$\boldsymbol{\mu}$	=	gyroscopic coupling torque, $\mathrm{N} \cdot \mathrm{m}$
ϕ	=	magnitude of Euler axis rotation, rad

$\boldsymbol{\omega}$ = spacecraft angular velocity, $\mathrm{m/s}$
ω_n = natural frequency of spacecraft, $1/\mathrm{s}$

1. INTRODUCTION

This research investigates the viability of using multiple small commercial-off-the-shelf (COTS) attitude determination and control systems (ADCS) to improve the performance of a 6U (10 x 20 x 30 cm) CubeSat. For convenience, the ADCS will be referred to as the "attitude control" subsystem or unit hereafter. As one of the most complex subsystems for all classes of satellite, attitude control subsystems require a specialized design in order to satisfy the control requirements for a given space mission and its constituent payload(s). The complexity of the attitude control subsystems usually leads spacecraft developers to purchase a COTS unit in order to reduce risk during both the pre-launch development and post-launch spacecraft operation. CubeSat-sized attitude control subsystems are typically manufactured to measure 0.5U (10 x 10 x 5 cm) and output a maximum of 900 mN·m of torque. Due to the non-custom nature of COTS attitude control units, however, CubeSat developers using large busses routinely utilize an attitude control subsystem with undersized reaction wheels for spacecraft control [1]. An undersized attitude control subsystem produces sub-optimal spacecraft performance which, in turn, decreases the operating potential of CubeSat payloads [2].

Numerous research studies have been conducted pertaining to 3-axis control using 3-wheel [3] and 4-wheel [4] reaction wheel assemblies. Some of the studies investigate time optimal control algorithms [5], while others focus on energy efficient control laws using both attitude regulation and tracking [6], or the use of reaction wheels for continuous momentum dumping [7]. Studies have also compared multiple control methods, to include proportional derivative and linear-quadratic regulator controllers, on the same spacecraft with the same maneuver [8]. Since the focus of this research is on multiple attitude control subsystems feasibility, it will utilize a simple proportional derivative control law using quaternion feedback linearization [9]. In contrast to these contemporary studies, the present research expands the number of potential attitude control units within the spacecraft and examines the coupling effects of two independent units to create a desired control response. Departing from the convention of a single unit for enabling attitude control, the use of multiple independent attitude control units may promote increased subsystem modularity and support accelerated spacecraft development via "plug-and-play" technology constructs [10], [11], [12].

The paper is structured with Section 2 defining the CubeSat system, attitude control units, and model assumptions underpinning the analysis. In Section 3, we discuss the formulation of the modular attitude control algorithm methodology with respect to a 6U-CubeSat chassis. Next, Section 4 provides the quaternion error for two attitude control units in three test cases, with each case featuring different spatial locations and torque orientations for the attitude control units. Section 5 presents a multi-objective optimization of attitude control units within a 6U-chassis, and, finally, Section 6 presents analysis conclusions.

2. SYSTEM DEFINITION AND SIMULATION ASSUMPTIONS

The attitude control units are constructed as "black box" systems within a generic 6U CubeSat chassis, with each unit featuring a unique (x, y, z) spatial offset from the CubeSat center-of-gravity (CG), and a control law utilizing a quaternion feedback regulator. The physical properties of the reaction wheels comprising each unit are representative of publically-available values for the Blue Canyon Technologies' XACT system, a contemporary attitude control unit employed by numerous on-orbit and legacy CubeSat missions [13]. Fixing each unit inside the 6U chassis is accomplished by constructing a motor-to-body (**MB**) torque distribution matrix from the wheel location properties and defining a generic pyramidal array assembly with four reaction wheels given as:

$$\mathbf{M_{EL}} = \left[\frac{20\pi}{180} \quad \frac{20\pi}{180} \quad \frac{20\pi}{180} \quad \frac{20\pi}{180}\right]^{\mathrm{T}}, \tag{1}$$

$$\mathbf{M_{AZ}} = \left[\frac{135\pi}{180} \quad \frac{225\pi}{180} \quad \frac{315\pi}{180} \quad \frac{45\pi}{180}\right]^{\mathrm{T}}, \tag{2}$$

$$\mathbf{MB} = \begin{bmatrix} r\cos(\mathbf{M_{EL}})\cos(\mathbf{M_{AZ}}) \\ r\cos(\mathbf{M_{EL}})\sin(\mathbf{M_{AZ}}) \\ r\sin(\mathbf{M_{EL}}) \end{bmatrix}, \tag{3}$$

where **MB** is a $[3 \times 4]$ is a mapping of wheel coordinates from spherical to three-dimensional Cartesian coordinates, and the radius r is assumed unity. The torque distribution matrix is then translated to the center of a particular CubeSat unit (U) with constant x, y, z offsets and rotated into a desired orientation with a rotation matrix in Eqs. (4)-(6), where θ is in increments of $(\pi/2)$ depending on the necessary rotation, and

$$\mathbf{R_x} = \begin{bmatrix} 1 & 0 & 0 \\ 0 & \cos\theta & -\sin\theta \\ 0 & \sin\theta & \cos\theta \end{bmatrix}, \tag{4}$$

$$\mathbf{R_y} = \begin{bmatrix} \cos\theta & 0 & -\sin\theta \\ 0 & 1 & 0 \\ \sin\theta & 0 & \cos\theta \end{bmatrix}, \tag{5}$$

$$\mathbf{R_z} = \begin{bmatrix} \cos\theta & -\sin\theta & 0 \\ \sin\theta & \cos\theta & 0 \\ 0 & 0 & 1 \end{bmatrix}. \tag{6}$$

Due to the four-wheel structure of each attitude control unit, **MB** is not a square matrix; as a result, the Moore-Penrose pseudo-inverse ($\mathbf{MB}^{+}$) is calculated using

$$\mathbf{MB}^{+} = \mathbf{MB}^{\mathrm{T}}(\mathbf{MB} \cdot \mathbf{MB}^{\mathrm{T}})^{-1}, \tag{7}$$

and divided by the wheel inertias (W**)** properties to provide a system-level moment of inertia (MOI) for the CubeSat and constituent attitude control units [14]. An example 6U CubeSat with two independent attitude control subsystems, with the respective orientations of each unit, is given in Fig. 1.

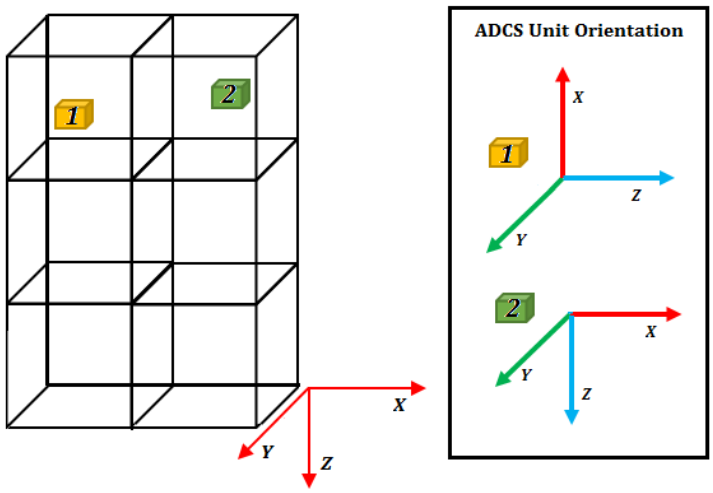

Fig. 1. Example Spatial Locations of Attitude Control Subsystem 1 and 2 inside a 6U CubeSat Rigid Body

The initial conditions for the system were chosen based on nominal, real-world conditions experienced by attitude control units by small satellites. The initial attitude quaternion q_0 was selected to be sufficiently far from the desired quaternion so as to provide a meaningful analysis of the input parameters into the modular attitude control subsystem model. Next, the initial wheel speeds $\boldsymbol{v_i}$ were varied within the interval $-S < \boldsymbol{v_i} < S, i = 1,2$, with the upper bound representing the wheel saturation speed [15]. The wheel saturation speed **S** is set to 700 rev/s. The saturation function is shown in Fig. 2, as well as

$$sat(\boldsymbol{v_i}) = \begin{cases} S & \text{if } \boldsymbol{v_i} > S \\ \boldsymbol{v_i} & \text{if } -S < \boldsymbol{v_i} < S. \\ -S & \text{if } \boldsymbol{v_i} < -S \end{cases} \tag{8}$$

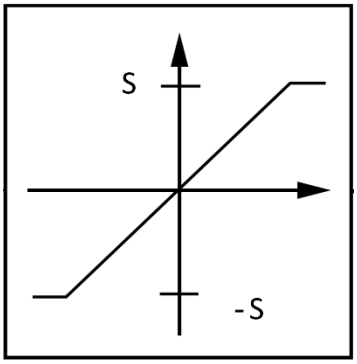

Fig. 2. Wheel Saturation Limits

Finally, the initial spacecraft angular velocity $\boldsymbol{\omega_0}$ was chosen close to the equilibrium condition corresponding to an "almost" stabilized system. The initial conditions for the attitude quaternion, wheel speeds, and spacecraft angular velocity are given by

$$\mathbf{q_0} = [0.59 \quad 0.59 \quad 0.59 \quad 0.157]^{\mathrm{T}}, \tag{9}$$

$$\boldsymbol{v1}_{s_0} = [675 \quad -675 \quad 675 \quad -675]^{\mathrm{T}}, \tag{10}$$

$$\boldsymbol{v2}_{s_0} = [75 \quad -75 \quad 75 \quad -75]^{\mathrm{T}}, \tag{11}$$

$$\boldsymbol{\omega_0} = [-0.05 \quad -0.05 \quad -0.05]^{\mathrm{T}}. \tag{12}$$

For model simplicity, the spacecraft system defines the CG at $(0,0,0)$, and the spacecraft MOI matrix is a uniform solid rectangle defined in

$$[\mathbf{I}] = \begin{bmatrix} (Y^2 + Z^2)/12 & 0 & 0 \\ 0 & (X^2 + Z^2)/12 & 0 \\ 0 & 0 & (X^2 + Y^2)/12 \end{bmatrix} \cdot m, \tag{13}$$

where the variables X, Y, and Z respectively represent the lengths of the sides of the CubeSat in meters, and m is the mass in kilograms. This research models a 6U CubeSat with sides of length $X = 0.2$, $Y = 0.1$, and $Z = 0.3$ m. The attitude control units are placed inside the spacecraft system at offsets from the system's MOI, the CG, corresponding to physical constraints of the chassis of (x ± 7.5 cm, y ± 2.5 cm, z ± 12.5 cm). Additionally, the units are considered massless. When unit is translated to a different U, the simulation does not adjust, but uses the same idealized uniform rectangle for all unit orientations. The torque distribution matrix is then generated with the pseudo-inversed motor-to-body torque distribution matrix and wheel inertias with

$$[\mathbf{J}] = \mathbf{M}\mathbf{B}^{+}/W. \tag{14}$$

Euler's equations of motion describe the rotation of a rigid body about body-fixed axes affixed to the center-of-mass. The general case is described by Eqn. (15), where $\boldsymbol{\Omega}$ is the skew-symmetric matrix in Eqn. (16) and $\mathbf{u}$ is the control torque vector,

$$[\mathbf{I}]\dot{\boldsymbol{\omega}} = -\boldsymbol{\Omega}[\mathbf{I}]\boldsymbol{\omega} + \mathbf{u}, \tag{15}$$

$$\boldsymbol{\Omega} = \begin{bmatrix} 0 & -\omega_3 & \omega_2 \\ \omega_3 & 0 & -\omega_1 \\ -\omega_2 & \omega_1 & 0 \end{bmatrix}. \tag{16}$$

The feedback controller for consists of linear error-quaternion feedback, linear body-rate feedback, and a nonlinear body-rate feedback term that counteracts the gyroscopic coupling torque. From Eqn. (15), the control torque vector $\mathbf{u}$ is given by

$$\mathbf{u} = \boldsymbol{\Omega}[\mathbf{I}]\boldsymbol{\omega} - \mathbf{D}\boldsymbol{\omega} - \mathbf{K}\mathbf{q_c}, \tag{17}$$

where $\mathbf{D}$ and $\mathbf{K}$ are $[3 \times 3]$ gain matrices selected to guarantee stability [16] and $\mathbf{q_c}$ is the commanded quaternion. The gain matrices $\mathbf{D}$ and $\mathbf{K}$ are defined in

$$\mathbf{K} = 2(\zeta\omega_n^2) \cdot [\mathbf{I}], \qquad \mathbf{D} = \sqrt{2\mathbf{K}}, \tag{18}$$

where ζ is the damping ratio and ω_n is the natural frequency. The controller was selected where the first term is nonlinear body-rate feedback and counteracts gyroscopic coupling in the wheels, the second term is for linear body-rate feedback, and the third term is for linear quaternion error feedback.

The four elements of the quaternion are defined in

$$\mathbf{q_i} = c_i \cos(\phi/2), \qquad i = 1,2,3, \tag{19}$$

$$q_4 = \cos(\phi/2), \tag{20}$$

where c_i are direction cosines of Euler axis relative to reference frame and ϕ is the magnitude of Euler axis rotation. The quaternion satisfies the relation in

$$1 = q_1^2 + q_2^2 + q_3^2 + q_4^2 = \|\mathbf{q}\|, \tag{21}$$

and creates the quaternion kinematic differential equations described by

$$\dot{\mathbf{q}} = \tfrac{1}{2}\boldsymbol{\Omega}\mathbf{q} + \tfrac{1}{2}q_4\boldsymbol{\omega}, \tag{22}$$

$$\dot{q}_4 = -\tfrac{1}{2}\boldsymbol{\omega}^{\mathrm{T}}\mathbf{q}. \tag{23}$$

A semi-analytical solution of the quaternion kinematic equation for deriving Eqn. (20) to Eqn. (23) can be found in the literature [17].

The stability of the independent closed-loop systems is investigated. Using Eqs. (14) and (16), we assume $0 < \mu < 1$, where $\mu = 1$ is the case when the gyroscopic torque is exactly countered by the control torque, and $\mu = 0$ is when the quaternion and linear rate feedback are used. That is,

$$[\mathbf{I}]\dot{\boldsymbol{\omega}} = -\boldsymbol{\Omega}[\mathbf{I}]\boldsymbol{\omega} - \mu\boldsymbol{\Omega}[\mathbf{I}]\boldsymbol{\omega} - \mathbf{D}\boldsymbol{\omega} - \mathbf{K}\mathbf{q_c}. \tag{24}$$

Since the gain matrices in Eqn. (18) were chosen in the given manner, we know $\mathbf{K^{-1}}$ exists and $\mathbf{K^{-1}}[\mathbf{I}]$ is positive definite. For simplicity, the commanded quaternion is assumed to be [0,0,0,1], which drives the error quaternion to be replaced by the current attitude quaternion. This allows us to replace $\mathbf{q_e}$ with the current attitude quaternion. Therefore, we define the Lyapunov candidate function

$$\begin{aligned} V &= \tfrac{1}{2}\boldsymbol{\omega}^{\mathrm{T}}\mathbf{K}^{-1}[\mathbf{I}]\boldsymbol{\omega} + q_1^2 + q_2^2 + q_3^2 + (q_4 - 1)^2 \\ &= \tfrac{1}{2}\boldsymbol{\omega}^{\mathrm{T}}\mathbf{K}^{-1}[\mathbf{I}]\boldsymbol{\omega} + 2(1 - q_4), \end{aligned} \tag{25}$$

and the simplified Lyapunov function is also positive definite and radially unbounded.

The time derivative of the Lyapunov function becomes

$$\dot{V} = \frac{1}{2}\dot{\boldsymbol{\omega}}^{\mathrm{T}}\mathbf{K}^{-1}[\mathbf{I}]\boldsymbol{\omega} + \frac{1}{2}\boldsymbol{\omega}^{\mathrm{T}}\mathbf{K}^{-1}[\mathbf{I}]\dot{\boldsymbol{\omega}} - 2\dot{q}_4 = \boldsymbol{\omega}^{\mathrm{T}}\mathbf{K}^{-1}[\mathbf{I}]\dot{\boldsymbol{\omega}} - 2\dot{q}_4 \tag{26}$$

$$= -\boldsymbol{\omega}^{\mathrm{T}}\mathbf{K}^{-1}\mathbf{D}\boldsymbol{\omega} + (1-\mu)\boldsymbol{\omega}^{\mathrm{T}}\mathbf{K}^{-1}\boldsymbol{\Omega}[\mathbf{I}]\boldsymbol{\omega} \tag{27}$$

$$= -\boldsymbol{\omega}^{\mathrm{T}}\mathbf{K}^{-1}\mathbf{D}\boldsymbol{\omega}. \tag{28}$$

Assuming that $\mathbf{K}^{-1}[\mathbf{I}] = (\mathbf{K}^{-1}[\mathbf{I}])^{\mathrm{T}}$, $\dot{\mathbf{V}}$ can be reduced along the system trajectory to Eqn. (27). Using the assumptions and derivations from [9], Eqn. (27) can be further reduced to Eqn. (28). V is positive definite and $\dot{V}$ is negative semidefinite, showing equilibrium stability if $\mathbf{K}^{-1}\mathbf{D} > \mathbf{0}$, and the selection of $\mathbf{K}$ and $\mathbf{D}$ in Eqn. (18) enables this condition.

To prove asymptotic stability about a commanded equilibrium point, LaSalle's invariance principle is used with the set

$$V_0 = \{\mathbf{q}, \boldsymbol{\omega} | \dot{V} = 0\}. \tag{29}$$

The largest invariant set M_{inv} in V_0 is found when

$$V_0 = \{\boldsymbol{\omega}(t) = 0\}, \forall t > 0, \tag{30}$$

$$\rightarrow \dot{\boldsymbol{\omega}}(t) = 0. \tag{31}$$

Using Eqn. (24), Eqn. (31) becomes

$$\dot{\boldsymbol{\omega}}(t) = 0 \rightarrow \mathbf{q_c}(t) = 0. \tag{32}$$

Thus, the largest invariant set M_{inv} in V_0 is the equilibrium point itself. Using Corollary 4.1, the equilibrium point of the closed-loop system is asymptotically stable [18]. As a note, Corollary 4.1 is actually the Barbashin and Krasovskii principle, which is a special case of the LaSalle invariance principle, but was proved before LaSalle proved the general case.

3. METHODOLOGY

In a typical CubeSat, a COTS attitude control unit is a calibrated "black box" that minimally interfaces with the rest of the CubeSat. This research replicated that behavior by implementing two independent units to act on the same CubeSat structure without sharing information between each other. The only characteristic shared between the individual units is their relative torque contribution on the system. A switch was devised to facilitate changing the control from using either one of the attitude control units, to using both simultaneously. Simulations were conducted to illustrate these different control states, and analysis of these results will be shown below. The full simulation setup is shown in Fig. 3.

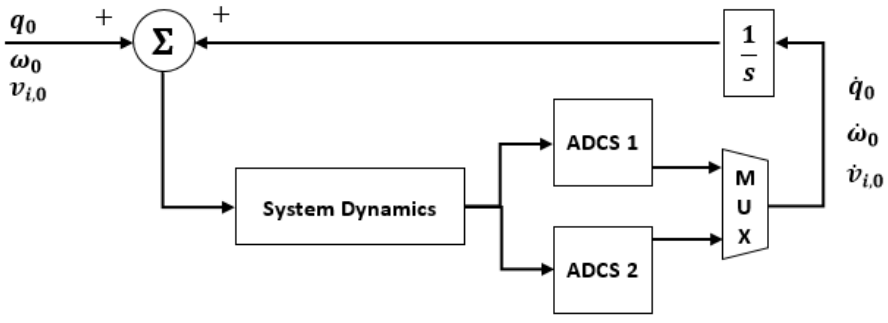

Fig. 3. Modular Attitude Control Subsystem Block Diagram

In Fig. 3, the initial conditions are set on the left, which initialize the attitude control subsystem pose, gain matrices, and identification of which attitude control unit will be run in the simulation. The initial conditions flow into each attitude control unit, where "ADCS 1" is given by the top block, and "ADCS 2" is the bottom block. The multiplexor on the bottom right will pass the $\dot{\boldsymbol{\omega}}$ contributions of the simulated attitude control units into the integrator. This switch keeps both units independent with their own controller calculations and only couple the units to the full system with their generated dynamics. For each unit, the wheel speeds $\mathbf{v_i}$ and motor torques $\mathbf{u_{s_i}}$ are calculated for each wheel; an example is shown in Fig. 4 with initial conditions defined by Eqs. (9)-(12) and the following desired final states:

$$\mathbf{q_f} = [0 \quad 0 \quad 0 \quad 1]^{\mathrm{T}}, \tag{33}$$

$$\boldsymbol{\omega_f} = [0 \quad 0 \quad 0]^{\mathrm{T}}. \tag{34}$$

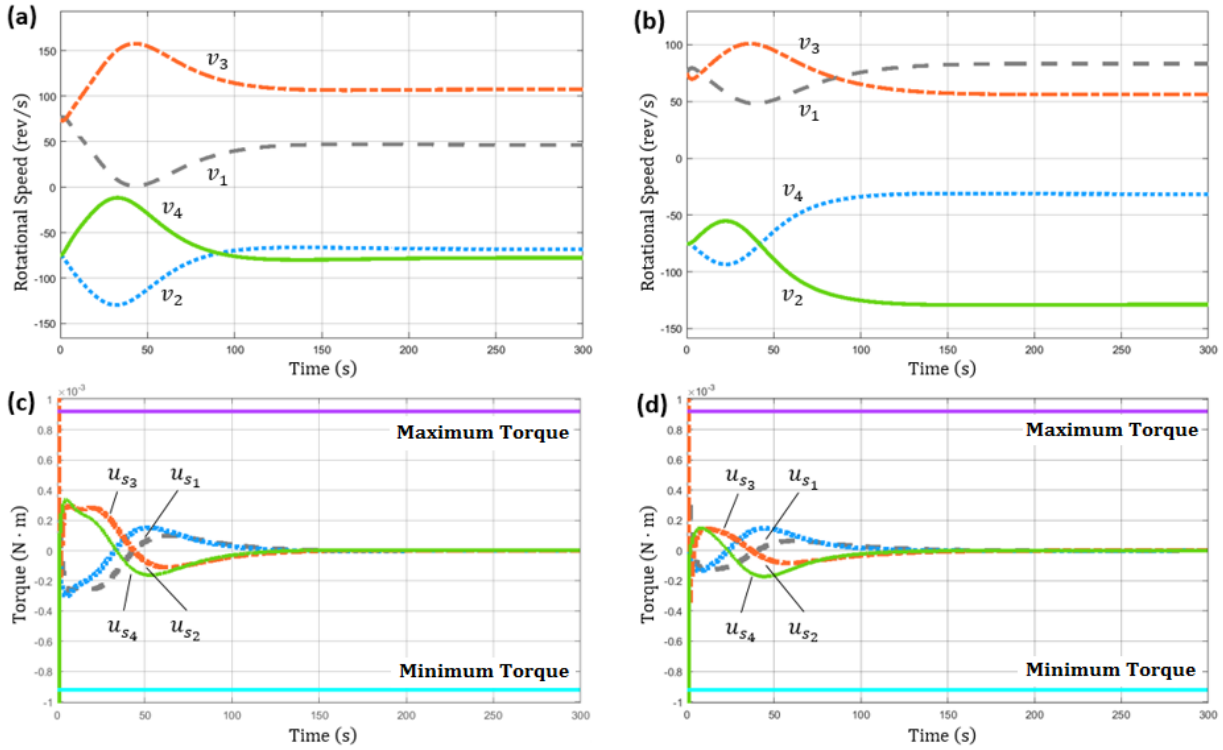

Fig. 4. Wheel Speeds and Motor Torques for Sample Simulation

The internal dynamics of each attitude control unit are shown in Fig. 5. The controller selected is the quaternion feedback linearization control law in Eqn. (17), and its implementation is relatively simple and straight forward. Each simulation step calculates the quaternion kinematics with

$$\dot{\mathbf{q}} = \begin{bmatrix} q_4 & -q_3 & q_2 & q_1 \\ q_3 & q_4 & -q_1 & q_2 \\ -q_2 & q_1 & q_4 & q_3 \\ -q_1 & -q_2 & -q_3 & q_4 \end{bmatrix}. \tag{33}$$

Simultaneously, the motor dynamics are run using the quaternion error from

$$\mathbf{q_c} = \begin{bmatrix} q_4 & q_3 & -q_2 & -q_1 \\ -q_3 & q_4 & q_1 & -q_2 \\ q_2 & -q_1 & q_4 & -q_3 \\ q_1 & q_2 & q_3 & q_4 \end{bmatrix}, \tag{34}$$

$$\mathbf{q_e} = \mathbf{q_c} \otimes \mathbf{q_i}, \tag{35}$$

then feeding it into the control law in Eqn. (17) to generate **u**. The control torques are distributed to each wheel with the spreading factor

$$\mathbf{Spread} = \frac{1}{4}\begin{bmatrix} -1 & 1 & -1 & 1 \\ 1 & -1 & 1 & -1 \\ -1 & 1 & -1 & 1 \\ 1 & -1 & 1 & -1 \end{bmatrix}, \tag{36}$$

along with Eqn. (17) and Eqn. (14) to generate $\dot{\boldsymbol{v}}$ using

$$\dot{\boldsymbol{v}} = [\mathbf{J}]\mathbf{u} + \left(\mathbf{Spread} \cdot ([\mathbf{J}]\mathbf{u} + \boldsymbol{v} - \boldsymbol{v_0})\right). \tag{37}$$

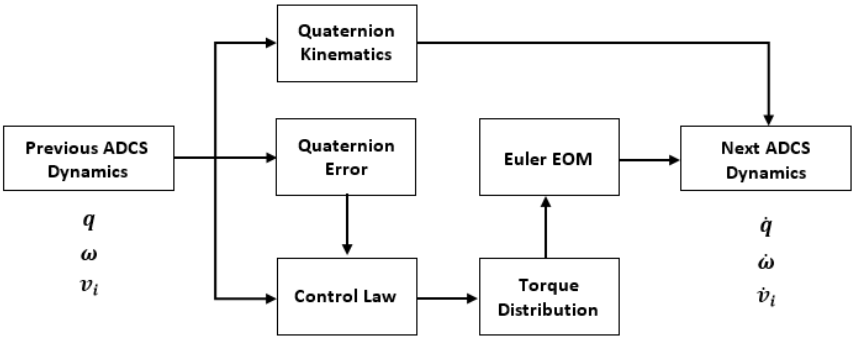

Fig. 5. Conceptual Attitude Control Subsystem Model

The system angular velocity is calculated by first finding the momentum required by each wheel with

$$\boldsymbol{h} = \boldsymbol{MB} \cdot \boldsymbol{v} \cdot W, \tag{38}$$

$$\boldsymbol{h_{cross}} = \boldsymbol{\omega} \times \boldsymbol{h}, \tag{39}$$

$$\dot{\boldsymbol{h}} = \boldsymbol{MB} \cdot \dot{\boldsymbol{v}} \cdot W, \tag{40}$$

where W is the wheel inertia. With **MB** being a $[3 \times 4]$ matrix and both $\boldsymbol{v}$ and $\dot{\boldsymbol{v}}$ are $[4 \times 1]$ vectors, **h** and $\dot{\mathbf{h}}$ will become $[3 \times 1]$ vectors. The wheel momentums are then run through the Euler equations of motion to generate $\dot{\boldsymbol{\omega}}$ using

$$\dot{\boldsymbol{\omega}} = [\mathbf{J}]/\left(\dot{\mathbf{h}} - \mathbf{h_{cross}} - \boldsymbol{\Omega}[\mathbf{J}]\boldsymbol{\omega}\right). \tag{41}$$

4. RESULTS AND ANALYSIS: TEST CASES

The primary focus of this section of the research is to determine if two independent COTS attitude control units are capable of constructively operating in conjunction within the same CubeSat chassis. If yes, then the amount of performance improvement compared with the operation of a single unit must be evaluated. The spatial and orientation conditions for the simulation cases presented herein are shown in Table 1. All cases were simulated based on the initial conditions and final states given by Eqs. (9)-(12) and Eqs. (33)-(34), respectively.

Table 1. Modular Attitude Control Test Case Definitions

Case Identification	ADCS Spatial Locations	ADCS Unit Orientation
Centered	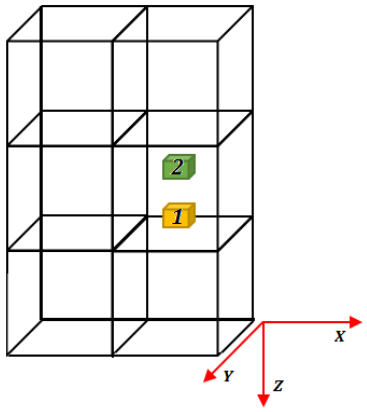	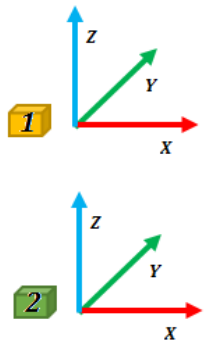
Corner	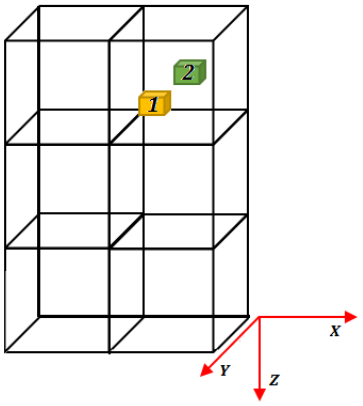	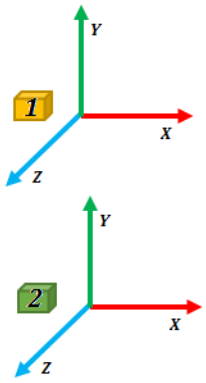
Opposite	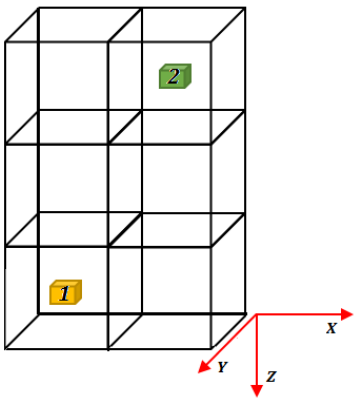	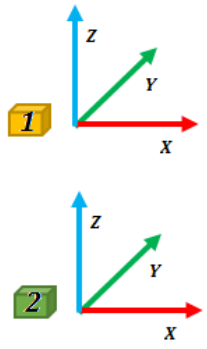

The initial simulation case focused on placing both units in the middle of the CubeSat and determine the difference between the same slew maneuver using only "ADCS 1," only "ADCS 2," and both "ADCS 1" and "ADCS 2" together. The initial conditions for this case are represented as the "Centered" case in This ADCS configuration is typically selected for CubeSat control, because the torque is located closest to the system's CG. The results in Fig. 6 show the quaternion error with the system for all three of these test cases. The red lines in Fig. 6 show the situation for using both units in the same test. Overall, Fig. 6 illustrates that the system settles on the desired quaternion at a faster rate with two units than either of the two single-operation cases. Also of note, the plots of "ADCS 1" and "ADCS 2" overlap in all three subplots, because they are using the same control law and have the same wheel torque properties. All MOI calculations use the same [**I**], but calculate a unique **MB** based on the attitude control subsystem pose.

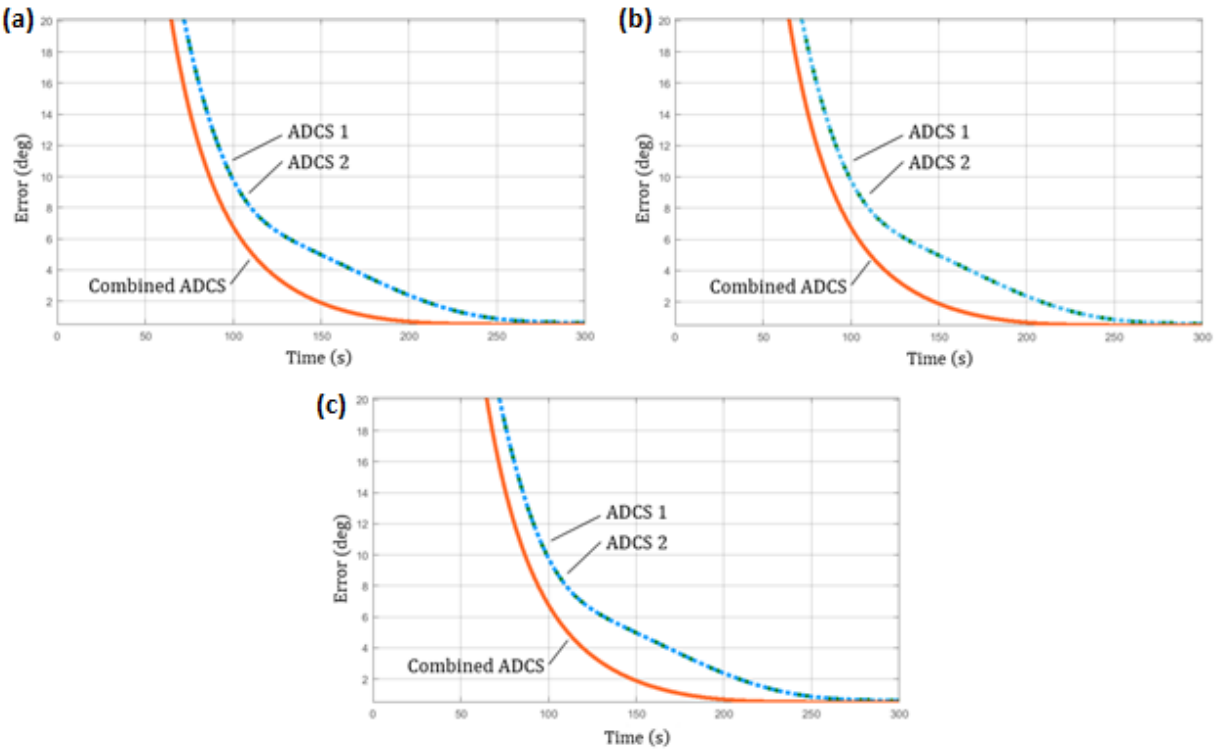

Fig. 6. (a) Results of Case 1 – Centered Attitude Control Subsystem; (b) Results of Case 2 – Corner Attitude Control Subsystem; and (c) Results of Case 3 – Opposite Attitude Control Subsystem

5. RESULTS AND ANALYSIS: MULTI-OBJECTIVE OPTIMIZATION

The cases discussed in Section 4 represent only aspect of the complete design space for a modular attitude control unit architecture. In addition to spatial placement and orientation of units within the bus, the number of units must be considered – whether two or more. These parameters represent factors that, in different combinations, provide a unique attitude control design. The next phase of analysis utilized the "Design of Experiments" (DOE) method of orthogonal arrays to provide optimal solutions based on the simulation of these attitude control designs, or experiments, arising from a user-defined design space associated with a multistate, multi-objective problem (MOP) [19]. In general, MOPs are characterized by competing objectives, in which the goal of the problem is to find the "best" solution that satisfies each objective. As a by-product of these competing objectives, there is frequently no single solution that emerges for an MOP but rather a family of solutions that represent an objective space [20], [21]. Based on the desire to minimize or maximize the given objectives, a Pareto front may form that shows a family of optimal solutions. A solution is determined to be on the Pareto front when it is non-dominated, or when no other feasible solution exists that improves both objective criteria. All other solutions outside of the Pareto front are considered dominated solutions, which prioritize one objective over the other objective [22]. Overall, DOE methods – specifically orthogonal arrays – have been utilized in disciplines such as biology and chemical engineering [23], as well as various aerospace optimization applications to include re-entry vehicle and trajectory design [24], [25].

For CubeSat attitude control design with modular units, the MOP is assumed to be constrained by the number of units that can fit inside of the available bus volume. Attitude determination and control represents but one subsystem for which the bus must provide spatial volume and power while also accommodating the payload and the remaining (and required) bus subsystems. Due to the volume constraints of a 6U chassis, the attitude control units are assumed to be 0.5U in size, with the total number of considered units being limited to 6 for the first case campaign, and 3 for the second. The former case represents an extremely over-actuated system, but represents an instructive maximum to discern control trends. Control response, power requirements, and heat generation signify design limitations that are considered once the requirements and capabilities of the payload and complete bus subsystems are known.

Given by Eq. (42), the MOP analysed herein seeks to minimize the settling time of the control response while minimizing the energy consumption of the attitude control units:

$$\text{MOP} = \begin{cases} \min E = f(\vec{x}) \\ \min t_s = f(\vec{x}) \end{cases} \\ \text{subject to} \quad \vec{x} \in [X_d, X_r] \tag{42}$$

where X_d and X_r represent the spatial location and axis orientation of each attitude control unit, respectively. For the first case campaign with up to 6 attitude control units possible, the total number of unit location/orientation permutations with the 6U bus was approximately 1.5 billion. Although exhaustive in its depiction of control possibilities, a campaign of such magnitude was judged too computationally extensive and, therefore, was reduced to 1000 location/orientation cases according Fig. 7:

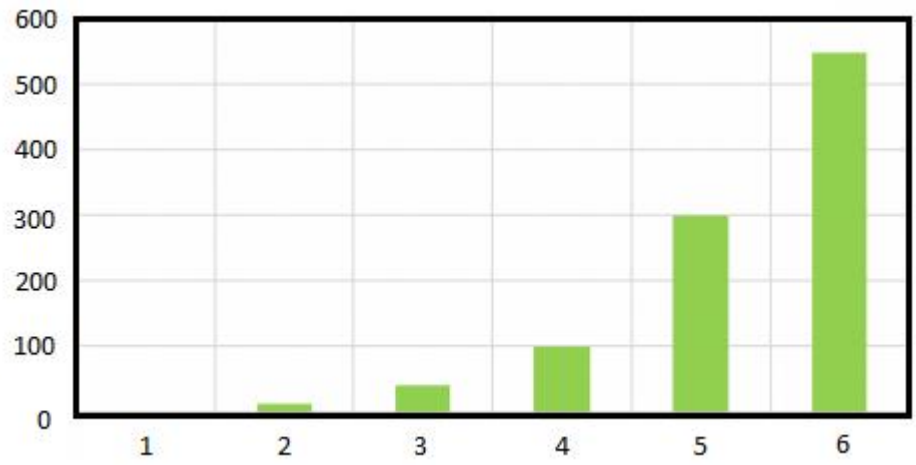

Fig. 7. Distribution of ADCS Units for 6-Unit Maximum Campaign

Fig. 8 illustrates the energy consumption versus settling time objective space of all experiments in the 6-unit maximum campaign based on the initial conditions given by Eqs. (9)-(12), as well as the desired final states shown by Eqs. (33)-(34). Of these results, only two attitude control unit configurations are deemed Pareto optimal and fulfilling the preceding MOP. Labeled as Points A and B in Fig. 8, these optimal solutions represent single unit cases rather than the use of up to 6 within a modular construct.

The same initial conditions and desired final states were used in the 3-unit maximum campaign which, in total, represented approximately 43,000 different cases, each featuring different spatial locations/orientations for up to 3 attitude control units within the 6U chassis Fig. 9 illustrates the energy consumption versus settling time objective space of these experiments, with only three attitude control unit configurations deemed Pareto optimal and fulfilling the preceding MOP. Labeled in the Fig. 9 inset as Points A, B, and C, the spatial locations/orientation of the attitude control units are outlined in Table 2. Of note, the optimal solutions indicate single units rather than the use of 2 or 3 within a modular construct. From these points, Point A corresponds with the lowest-settling time, C is the lowest energy consumption, while B is the configuration fully satisfying the MOP.

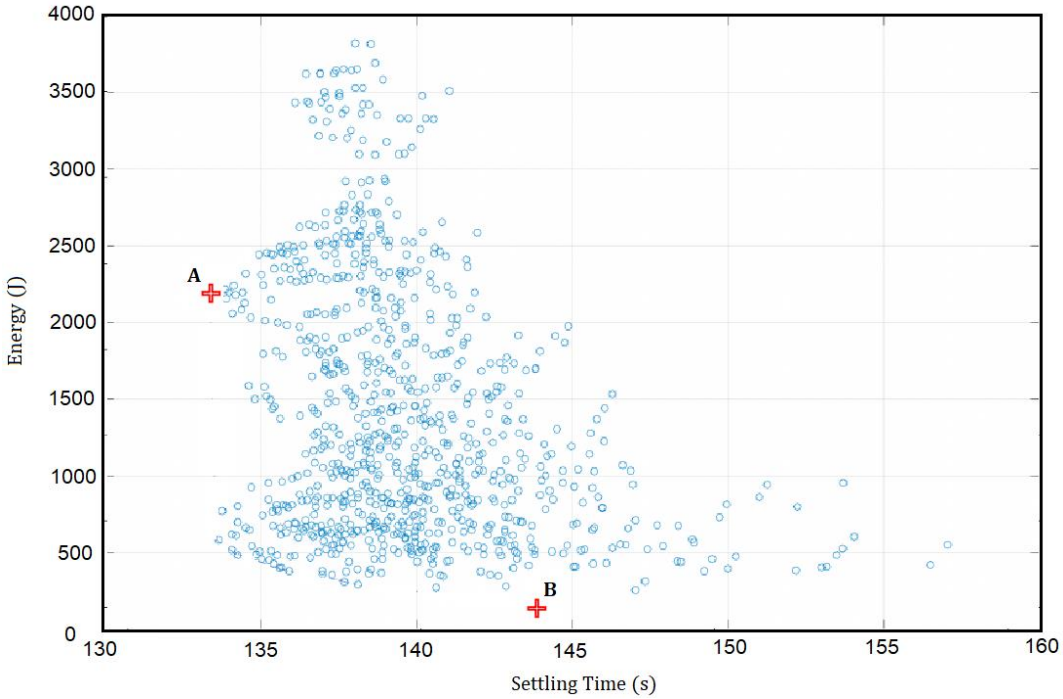

Fig. 8. 6-Unit Maximum Campaign: Objective Space and Selected Pareto Optimal Points for MOP $\{\min t_s, \min E\}$

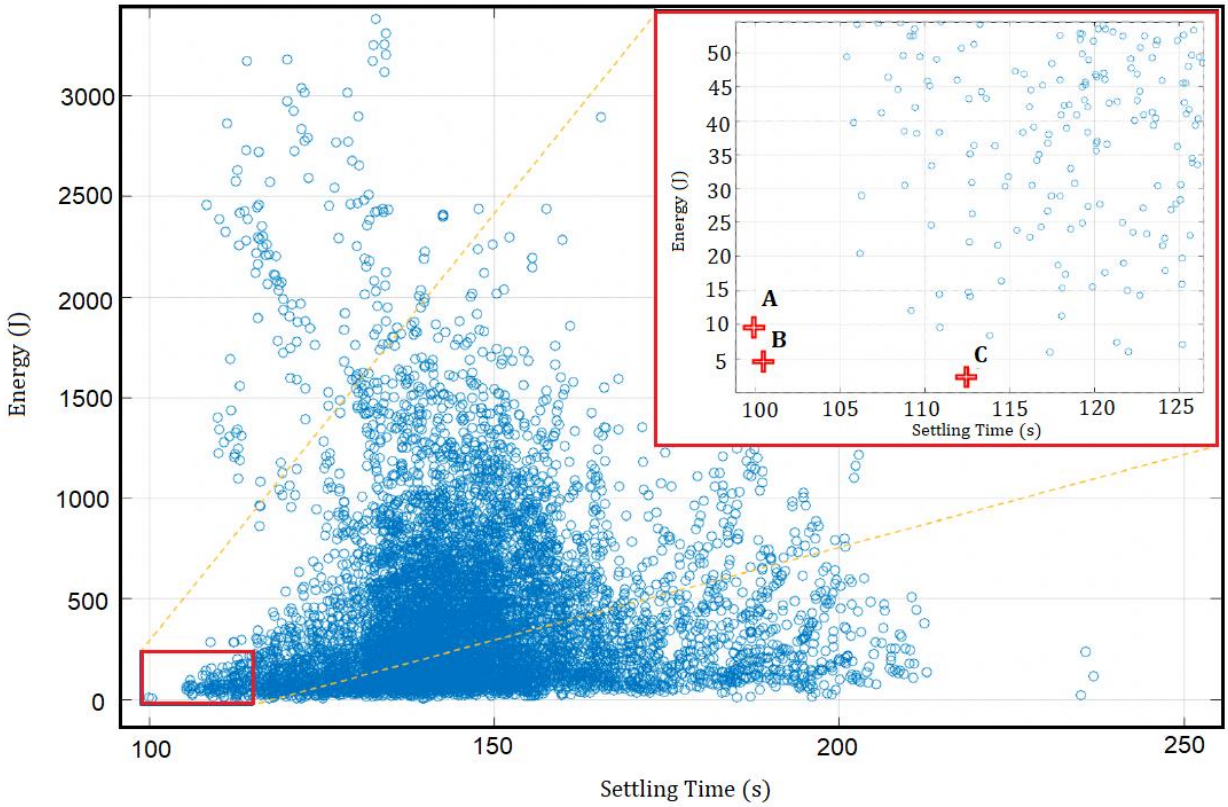

Fig. 9. 3-Unit Maximum Campaign: Objective Space and Selected Pareto Optimal Points for MOP $\{\min t_s, \min E\}$

Table 2. Optimal Solution Cases

Point Identification	ADCS Spatial Locations	ADCS Unit Orientation
A (Lowest Energy)	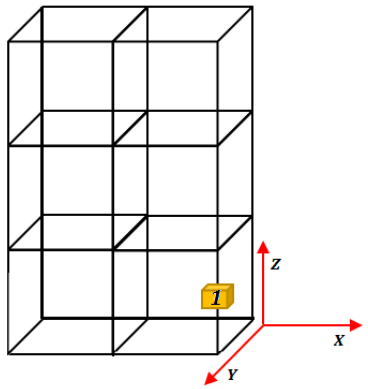	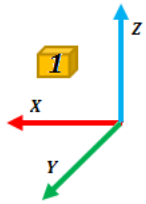
B (Pareto Optimal)	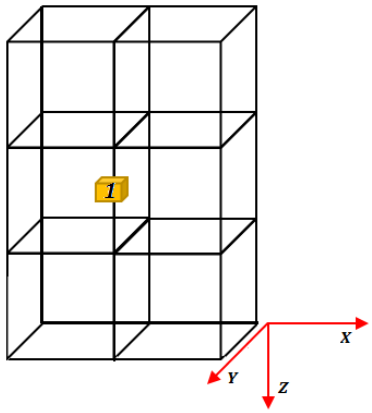	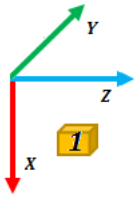
C (Lowest Settling Time)	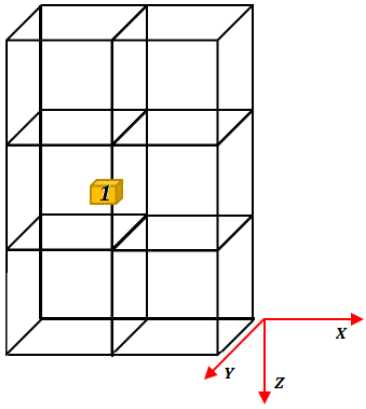	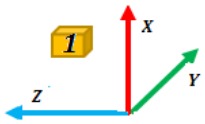

6. CONCLUSION

This research demonstrated that two independent COTS attitude control units can work in tandem to control a 6U CubeSat. For three example locations and orientations of the attitude control units within the CubeSat chassis, the combined operation of two units was shown to decrease the quaternion error at a faster rate than the operation of a single unit. As expected, the operation of two or more units generally required more energy than the single unit cases. From the test cases selected, however, the placement of units in one of the CubeSat corners generally resulted in a

lower energy consumption based on the given initial conditions and desired final end states. This research presents a new method by which to control CubeSats, with the use of multiple COTS attitude control units providing a viable control alternative to designing a custom, mission-dependent attitude control solution, or settling for a sub-optimal control solution with the use of only a single attitude control unit. Although compelling, the test cases presented herein represent only a cursory examination into the potential control authority afforded by multiple, yet independent attitude control units for CubeSats. Additional research will focus on conducting additional spatial placement and unit orientations studies within not only a 6U CubeSat, but also larger 12U- and 27U-chassis designs.

7. REFERENCES

[1] X. Cao, C. Yue, M. Liu, and B. Wu. Time Efficient Spacecraft Maneuver Using Constrained Torque Distribution, *Acta Astronautica*, 123: 320-329, 2016. doi:10.1016/J.ACTAASTRO.2016.03.026

[2] Z. Ismail and R. Varatharajoo. A Study of Reaction Wheel Configurations for a 3-Axis Satellite Attitude Controller, *Advances in Space Research*, 45(6): 750–759, 2010. doi:10.1016/j.asr.2009.11.004

[3] W. Steyn. Near-Minimum-Time Eigenaxis Rotation Maneuvers Using Reaction Wheels, *Journal of Guidance, Control, and Dynamics*, 18(5): 1184-1189, 1995. doi:10.2514/3.21523

[4] N. S. Bedrossian, J. Paradiso, E. V. Bergmann, and D. Rowell. Steering Law Design for Redundant Single-Gimbal Control Moment Gyroscopes, *Journal of Guidance, Control, and Dynamics*, Vol. 13(6), pp. 1083-1089, 1990. doi:10.2514/3.20582

[5] D. Verbin, V. J. Lappas, and J. Z. Ben-Asher. Time-Efficient Angular Steering Laws for Rigid Satellite, *Journal of Guidance, Control, and Dynamics*, 34(3): 878-892, 2011. doi:10.2514/1.48154

[6] R. Blenden and H. Schaub. Regenerative Power-Optimal Reaction Wheel Attitude Control, *Journal of Guidance, Control, and Dynamics*, 35(4), pp. 1208-1217, 2012. doi:10.2514/1.55493

[7] E. A. Hogan and H. Schaub. Three-Axis Attitude Control Using Redundant Reaction Wheels with Continuous Momentum Dumping, *Journal of Guidance, Control, and Dynamics*, 38(10): 1865–1871, 2015. doi:10.2514/1.g000812

[8] C-H. Won. Comparative Study of Various Control Methods for Attitude Control of a LEO Satellite, *Aerospace Science and Technology*, 3(5): 323–333, 1999. doi:10.1016/s1270-9638(00)86968-0

[9] B. Wie, H. Weiss, and A. Arapostathis. Quaternion Feedback Regulator for Spacecraft Eigenaxis Rotations, *Journal of Guidance, Control, and Dynamics*, 12(3): 375-380, 1989. doi:10.2514/3.20418

[10] P. Graven, Y. Plam, L. J. Hansen, and S. Harvey. Implementing Plug-and-Play ADCS to Support Operationally Responsive Space, presented at the 2008 IEEE Aerospace Conference, Big Sky, MT, March 2008. doi:10.1109/AERO.2008.4526507

[11] L. J. Hansen, J. Pollack, P. Graven, and Y. Plam. Plug-and-Play for Creating 'Instant' GN&C Solutions, presented at the 21st Annual AIAA/USU Conference on Small Satellites, Logan, UT, August 2007.

[12] L. J. Hansen, P. Graven, D. Fogle, and D. Lyke. The Feasibility of Applying Plug-and-Play Concepts to Spacecraft Guidance, Navigation, and Control Systems to Meet the Challenges of Future Responsive Space Missions, presented at the 7th International ESA Conference on Guidance, Navigation & Control Systems, Tralee, Ireland, June 2008.

[13] Blue Canyon Technologies: BCT News. "Blue Canyon Technologies Supports Multiple Missions on Spaceflight Industries' SSO-A Launch," http://bluecanyontech.com/blue-canyon-technologies-supports-multiple-missions-spaceflight-industries-sso-launch/ (accessed 13 March 2019).

[14] F. L. Markley, R. G. Reynolds, F. X. Liu, and K. L. Lebsock. Maximum Torque and Momentum Envelopes for Reaction Wheel Arrays, *Journal of Guidance, Control, and Dynamics*, 33(5): 1606-1614, 2010. doi:10.2514/1.47235

[15] H. Bang, M-J. Tahk, and H-D. Choi. Large Angle Attitude Control of Spacecraft with Actuator Saturation, *Control Engineering Practice*, 11(9): 989–1007, 2003. doi:10.1016/s0967-0661(02)00216-2

[16] J. Jin, S. Ko, and C-K. Ryoo. Fault Tolerant Control for Satellites with Four Reaction Wheels, *Control Engineering Practice*, 16(10): 1250-1258, 2008. doi:10.1016/j.conengprac.2008.02.001

[17] T. R. Kane. Solution of Kinematical Differential Equations for a Rigid Body, *Journal of Applied Mechanics*, 40(1): 109-113, 1973. doi:10.1115/1.3422907

[18] K. H. Khalil. *Nonlinear Systems*, 3rd ed., Upper Saddle River, NJ: Prentice Hall, 2002.

[19] E-G. Talbi. *Metaheuristics: From Design to Implementation*, Hoboken, NJ: John Wiley & Sons, Inc., 2009.

[20] P. Ngatchou, A. Zarei, and M. A. El-Sharkawi. Pareto Multi Objective Optimization, *Proceedings of the 13th International Conference on Intelligent Systems Application to Power Systems, ISAP'05*, 2005: 84–91, 2005.doi: 10.1109/ISAP.2005.1599245

[21] R. T. Marler and J. S. Arora. Survey of Multi-Objective Optimization Methods for Engineering, *Structural and Multidisciplinary Optimization*, 26(6): 369–395, 2004. doi: 10.1007/s00158-003-0368-6

[22] C. A. Coello Coello. Evolutionary Multi-Objective Optimization: A Historical View of the Field, *IEEE Computational Intelligence Magazine*, 1(1): 28–36, 2006. doi: 10.1109/MCI.2006.1597059

[23] T. Lundstedt, E. Seifert, L. Abramo, B. Thelin, A. Nyström, J. Petterson, and R. Bergman. Experimental Design and Optimization, *Chemometrics and Intelligent Laboratory Systems*, 42(1-2): 3-40, 1998.

[24] K. Daryabeigi. Thermal Analysis and Design of Multilayer Insulation for Re-Entry Aerodynamic Heating, *Journal of Spacecraft and Rockets*, 39(4): 509-514, 2002.doi: 10.2514/2.3863

[25] R. A. Bettinger, J. T. Black, and J. S. Agte. Design of Experiment Approach to Atmospheric Skip Entry Maneuver Optimization, *Journal of Spacecraft and Rockets*, 52(3): 813-826, 2015. doi: 10.2514/1.A333032